SOME REFLECTIONS ON DOUBLE NEGATIVE MATERIALS

W. C. Chew

Center for Computational Electromagnetics and
Electromagnetics Laboratory
Department of Electrical and Computer Engineering
University of Illinois at Urbana-Champaign
Urbana-Champaign, IL 61801-2991, USA [†]

Abstract—We study the energy conservation property and loss condition of a left-handed material (LHM). First we argue by energy conservation that an LHM has to be a backward-wave material (BWM). Then we derive the equivalence of the loss and the Sommerfeld far-field radiation conditions for BWM. Next, we solve the realistic Sommerfeld problem of a point source over an LHM half space and an LHM slab. With this solution, we elucidate the physics of the interaction of a point source with an LHM half space and an LHM slab. We interpret our observation with surface plasmon resonance at the interfaces as well as the resonance tunneling phenomenon. This analysis lends physical insight into the interaction of a point source field with an LHM showing that super-resolution beyond the diffraction limit is possible with a very low loss LHM slab.

1   Introduction

2   Symmetry in Physical Laws

3   Left-Handed Vacuum versus Right-Handed Vacuum

4   Mixing of LHV and RHV

5   Frequency Dispersive Left-Handed Material

6   Far Field Radiation and Loss Conditions for BWM

7   Point Source over an LHM Half Space

[†] Most of this work was done while the author was an IPA at AFRL, Dayton, OH, during Fall 2003. Part of the result was presented at PIERS 2003, Hawaii.

1. INTRODUCTION

There has been much recent interest in novel materials. The potential for fabricating novel materials at optical wavelength also looms larger than ever before, due to progress in fabrication technology and nano-technology. Many conjectures have been made about these novel materials [1–20].

A material of particular interest is the double negative material where both μ and ϵ are negative [1]. There are issues about the realizability of such a material, the ability to provide super-resolution, its time-reversal property and so on. We will address some of these issues in this paper.

2. SYMMETRY IN PHYSICAL LAWS

It was once thought that the laws of physics do not change under reflection, namely, that a physical law remains unchanged in the mirrored world as in the real world. This fact was known as the conservation of parity. The conservation of parity also implies that there is no preferred right-handedness or left-handedness in physical laws [21].

Take for example, the laws of electromagnetics: the fact that we have used right-hand rule in describing these laws is strictly by convention. Also, there are vectors known as pseudo vectors (or axial vectors) whose sign is strictly defined by convention. For instance, the direction of the $\boldsymbol{B}$ field, which is defined to point from the north pole to the south pole, is strictly by convention. Hence, the laws of electromagnetics could have been written with a left-hand rule with the sign of magnetic field changed. There is no preference for right-handedness or left-handedness for the laws of electromagnetics. We

can see this further by looking at Maxwell-Heaviside equations:

$$\nabla \times \boldsymbol{E} = -\mu_0 \frac{\partial \boldsymbol{H}}{\partial t}$$
$$\nabla \times \boldsymbol{H} = \epsilon_0 \frac{\partial \boldsymbol{E}}{\partial t} + \boldsymbol{J} \qquad (1)$$
$$\nabla \cdot \epsilon_0 \boldsymbol{E} = \rho$$
$$\nabla \cdot \mu_0 \boldsymbol{H} = 0$$

From the above, we can see that if the right-hand rule is replaced by the left-hand rule, the sign change can be rectified by changing the sign of the magnetic field $\boldsymbol{H}$.

Even though the laws of electromagnetics satisfy parity, there are some laws of weak decay that do not [22]. Hence, parity is not truly conserved, and some laws of physics have the preference for right-handedness or vice versa. However, it is believed by physicists that for every matter that exists in our real world, there is also an antimatter counterpart, an example of which is the positron versus electron–positron is the antimatter of electron. If our world prefers right-handedness, then the world of antimatter prefers left-handedness [21].

3. LEFT-HANDED VACUUM VERSUS RIGHT-HANDED VACUUM

Let us assume that a vacuum exists such the the signs of ϵ_0 and μ_0 are opposite to those of ours. If we were to change the sign of ϵ_0 and μ_0 in Equations (1), we arrive at:

$$\nabla \times \boldsymbol{E} = \mu_0 \frac{\partial \boldsymbol{H}}{\partial t}$$
$$\nabla \times \boldsymbol{H} = -\epsilon_0 \frac{\partial \boldsymbol{E}}{\partial t} + \boldsymbol{J} \qquad (2)$$
$$\nabla \cdot \epsilon_0 \boldsymbol{E} = -\rho$$
$$\nabla \cdot \mu_0 \boldsymbol{H} = 0$$

Once a solution to Equations (1) is obtained, we can obtain a solution to Equations (2) from the first solution by changing the sign of $\boldsymbol{H}$, $\boldsymbol{J}$, and ρ. Hence power flow, which is defined to be $\boldsymbol{E} \times \boldsymbol{H}$, points in the opposite direction for solutions of Equations (2) compared to that of solutions of Equations (1), or the left-hand rule has to be applied to get the correct direction of power flow. We shall call this medium a left-handed vacuum (LHV) and the conventional vacuum the right-handed vacuum (RHV). Notice that in an LHV, the sign of charge or

current has to change as well. This seems to agree with the assertion by physicists that in the world of antimatters, electrons become positrons, and a right-handed world becomes a left-handed world [21].

4. MIXING OF LHV AND RHV

In a vacuum, ϵ_0 and μ_0 are independent of frequency. An interesting question to ask is if an LHV can coexist with an RHV, i.e., can space be filled with non-overlapping LHV regions and RHV regions? A conservation law for power flow can be easily derived for a source-free region to be:

$$\nabla \cdot (\boldsymbol{E} \times \boldsymbol{H}) = -\frac{1}{2}\frac{\partial}{\partial t}\{\mu|\boldsymbol{H}|^2 + \epsilon|\boldsymbol{E}|^2\} \tag{3}$$

or in integral form via the use of Gauss' divergence theorem:

$$\oint_S d\boldsymbol{S} \cdot (\boldsymbol{E} \times \boldsymbol{H}) = -\frac{1}{2}\frac{\partial}{\partial t}\int_V dV\{\mu|\boldsymbol{H}|^2 + \epsilon|\boldsymbol{E}|^2\} \tag{4}$$

In the above, when LHV and RHV co-exist and mix with each other, ϵ and μ can have different signs for different regions. Hence, with a proper choice of surface and volume, the right-hand side of the above can be zero, while the left-hand side is non-zero violating energy conservation! Hence, we cannot mix an LHV with an RHV without violating energy conservation unless sources and sinks are added at the interfaces between these vacuums.

This problem can be further clarified by constructing the following thought experiment: the case of a plane electromagnetic wave incident at a planar interface between an RHV and an LHV. For simplicity, we consider a normally incident plane wave. For a source free vacuum, a plane wave solution where the fields are proportional to $\exp(i\boldsymbol{k} \cdot \boldsymbol{r})$ can be easily obtained for both Equations (1) and (2). In this case,

$$k = \pm\omega\sqrt{\mu_0\epsilon_0} \tag{5}$$

It is also seen that the group velocity and the phase velocity are frequency independent.

On the left-hand side, we have an RHV, and the steady-state, time-harmonic solution of a normally incident wave is:

$$\boldsymbol{E} = \hat{x}E_0e^{ikz} \tag{6}$$

$$\boldsymbol{H} = \hat{y}\frac{E_0}{\eta}e^{ikz} \tag{7}$$

where $k = \omega\sqrt{\mu_0\epsilon_0} > 0$, assuming $e^{-i\omega t}$ time dependence.

On the right-hand side, we have an LHV, and in order to match the boundary condition of continuity of tangential $\boldsymbol{E}$ and tangential $\boldsymbol{H}$ field, the steady-state, time-harmonic solution of a normally incident wave is:

$$\boldsymbol{E} = \hat{x}E_0 e^{-ikz} \tag{8}$$

$$\boldsymbol{H} = \hat{y}\frac{E_0}{\eta}e^{-ikz} \tag{9}$$

One can show from Maxwell-Heaviside equations that for such half spaces, tangential $\boldsymbol{E}$ and tangential $\boldsymbol{H}$ are still continuous across a source-free interface. Furthermore, one can add a reflected wave to the incident wave above, and easily show that the reflected wave is zero. Nevertheless, the above fields alone satisfy the boundary condition.

Since the above solution, being a solution in a non-dispersive vacuum, is valid for all frequencies, we can easily Fourier transform the above solution to form a time-domain solution. The time-domain counterpart of the above solution corresponds to two identical pulses travelling to the boundary and disappearing as shown in the top part of Figure 1.
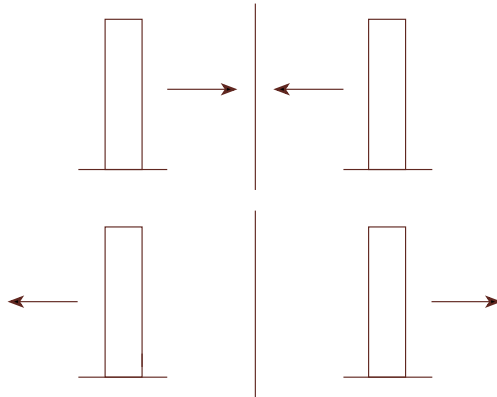

Figure 1. At an LHV/RHV interface, two pulses can move toward the interface and annihilate each other, or two pulses can be spontaneously generated at the interface and move away from the interface. These solutions violate energy conservation in the traditional sense.

Another way to set up a solution that satisfies the boundary condition is to switch the signs of k and $\boldsymbol{H}$ in the above solution. Again, the time-domain counterpart of this solution corresponds to

two identical pulses emerging from the boundary, and travelling away from the boundary (see the bottom part of Figure 1).

Both the above solutions violate energy conservation. However, if we postulate that sources and sinks exist at the interface between LHV and RHV, energy conservation law need not be violated.

5. FREQUENCY DISPERSIVE LEFT-HANDED MATERIAL

In the above example, we see that if a left-handed material (LHM) is non-dispersive, the group velocity (energy velocity) is in the same direction as the phase velocity, giving rise to irreconcilable violation of energy conservation. It has been known that negative μ and negative ϵ material (double negative material) can be constructed over a finite bandwidth of frequency [3]. If the group velocity and the phase velocity of such material are in the same direction, we can construct the same thought experiment as in the previous section, where two narrow band pulses will disappear into an interface or emerging spontaneously from an interface, violating energy conservation.

In order not to violate energy conservation, it is necessary that such frequency dispersive LHM have group velocity in the opposite direction to that of the phase velocity. Such material is also known as a backward wave material (BWM). (However, not all backward waves have to come from LHM, as is obviated in photonic band gap structures — photonic band gap structures can produce a backward wave with group velocity opposite in direction the phase velocity by using an array of interfering rods and objects.)

At a planar interface between and LHM and RHM, the $\boldsymbol{k}$ vectors represent the directions of the phase velocities, and in order for energy to be conserved, they have to point toward the interface so that in the LHM (also a BWM), energy will flow away from the interface. Together with the phase-matching condition, this gives rise to the phenomenon of negative refraction (see Figure 2). It is to be noted that the phenomenon of negative refraction is due to the backward wave nature, and not restricted to the left-handed nature of the material. In other words, non-LHM with backward wave phenomenon also exhibits negative refraction.

6. FAR FIELD RADIATION AND LOSS CONDITIONS FOR BWM

The far field radiation condition, also known as the Sommerfeld radiation condition, for an unbounded conventional medium is well
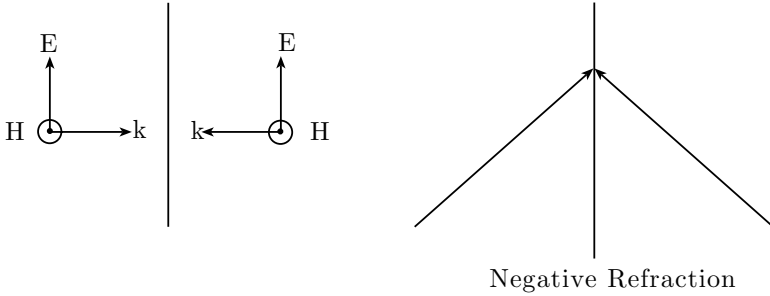
Negative Refraction

Figure 2. Negative refraction at an RHM/LHM interface is entirely due to the backward wave nature of one of the media, and is not a property restricted to LHM.

known [24, p. 35]. It is required to guaranteed uniqueness in a solution in an unbounded region. The far-field condition for a lossless medium can be derived by first introducing an infinitesimal amount of loss in the medium, and finally letting the amount of loss vanish. In the limit of vanishing loss, the far field condition is also the same as an outgoing wave condition [24, p. 35]. The outgoing wave corresponds to the convection of energy to infinity. This outgoing wave condition is often expressed as an impedance-like boundary condition in the far field

$$\lim_{r \to \infty} r \left[\frac{\partial \phi(\boldsymbol{r})}{\partial r} - ik\phi(\boldsymbol{r}) \right] = 0 \tag{10}$$

However, the far field condition in the past has always been derived assuming that we have a medium where the group and phase velocities are in the same direction. In the case of LHM or BWM, the phase and the group velocities have to be opposite in their directions. In such a medium, a finite size source that produces a wave that carries energy to infinity has to be proportional to a spherical wave of the form

$$\frac{e^{-ikr}}{r} \tag{11}$$

for $e^{-i\omega t}$ dependence. Therefore, when there is a small amount of loss in the unbounded BWM, this wave has to vanish at infinity. This gives rise to the following condition for loss

$$k = k' - ik'' \tag{12}$$

where the imaginary part of k has to be negative. The corresponding

impedance boundary condition at infinity is

$$\lim_{r \to \infty} r \left[\frac{\partial \phi(\boldsymbol{r})}{\partial r} + ik\phi(\boldsymbol{r}) \right] = 0 \tag{13}$$

We can also obtain the loss condition from complex Poynting theorem in the frequency domain which reads

$$\oint_S d\boldsymbol{S} \cdot (\boldsymbol{E} \times \boldsymbol{H}^*) = i\omega \int_V dV \{\mu|\boldsymbol{H}|^2 + \epsilon|\boldsymbol{E}|^2\} \tag{14}$$

In an LHM when μ and ϵ are complex corresponding to lossy media, we assume them to be of the form $\mu = -\mu' + i\mu''$ and $\epsilon = -\epsilon' + i\epsilon''$ where μ', μ'', ϵ' and ϵ'' are all positive real numbers. When the complex μ and ϵ are substituted into (14), the resultant equation is

$$\oint_S d\boldsymbol{S} \cdot (\boldsymbol{E} \times \boldsymbol{H}^*) = -i\omega \int_V dV \{\mu'|\boldsymbol{H}|^2 + \epsilon'|\boldsymbol{E}|^2\} - \omega \int_V dV \{\mu''|\boldsymbol{H}|^2 + \epsilon''|\boldsymbol{E}|^2\} \tag{15}$$

The first integral on the right-hand side represents the reactive energy stored in the field which is purely imaginary, and hence does not contribute to the real part of the complex Poynting power. The second integral represents the energy absorbed by the lossy medium, which by energy conservation, has to be negative to represent a net energy flow into the volume V. Therefore, even when the real parts of μ and ϵ are negative, their imaginary parts have to be positive in order to conserve energy and our assumption right after Equation (14) is correct.

When the above form of μ and ϵ are used to compute k via the formula

$$k = \pm\omega\sqrt{\mu\epsilon} = \pm\omega\sqrt{(\mu' - i\mu'')(\epsilon' - \epsilon'')} \tag{16}$$

It is clear from the above that when the branch of the square root is chosen so that the real part of k is positive, the imaginary part of k has to be negative as suggested by Equation (12). This loss condition is also in agreement with that in [10] via a more elaborate argument.

7. POINT SOURCE OVER AN LHM HALF SPACE

The solution of a point source over an LHM half space can be solved in closed form in terms of Sommerfeld integrals. The Sommerfeld integrals provide an excellent theoretical model that allows us to elucidate the physics of the problem, and gain further insight into the physical interaction of a source with an LHM half space and later, an LHM slab.
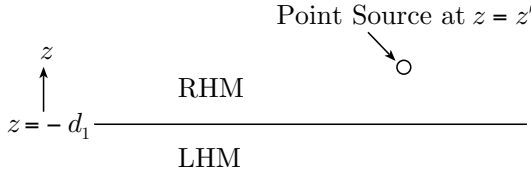
Point Source at $z = z'$

z

RHM

$z = -d_1$ ———————————————————————

LHM

Figure 3. A point source over an LHM half space. The point source is located in the upper half space which is an RHM.

Without loss of generality, we consider the case of a vertical electric dipole on top of a half space where the upper half space is vacuum while the lower half space is an LHM (see Figure 3). The field generated by such a dipole is transverse magnetic with respect to z, the vertical axis. (If transverse electric field is desired, one can use a vertical magnetic dipole. But the physics of the problem is not greatly altered by polarization.) In the upper half space, the z component of the electric field can be expressed as [23, 24]

$$E_{1z} = -\frac{I\ell}{4\pi\epsilon_1} \int_0^\infty dk_\rho \frac{k_\rho^3}{k_{1z}} J_0(k_\rho \rho) \left[e^{ik_{1z}|z-z'|} + Re^{ik_{1z}(z+d_1+|d_1+z'|)} \right]$$
(17)

where the source is located at $\rho = 0$ and $z = z'$, while the interface is located at $z = -d_1$. In the lower half space, it is

$$E_{2z} = -\frac{I\ell}{4\pi\epsilon_1} \int_0^\infty dk_\rho \frac{k_\rho^3}{k_{1z}} J_0(k_\rho \rho) Te^{ik_{1z}|d_1+z'|-ik_{2z}(z+d_1)}$$
(18)

where

$$R = \frac{\epsilon_2 k_{1z} - \epsilon_1 k_{2z}}{\epsilon_2 k_{1z} + \epsilon_1 k_{2z}}; \quad T = 1 + R$$
(19)

In the above,

$$k_{iz} = \sqrt{k_i^2 - k_\rho^2}; \quad k_i^2 = \omega^2 \mu_i \epsilon_i$$
(20)

for the i-th region.

The above integrals are not uniquely defined until the branch of the square root in k_{iz} is specified. There will be four branch points corresponding to $\pm k_i$, $i = 1, 2$ for the above problem. To obtain a unique solution to the above problem, an infinitesimal small loss is first assumed in its formulation, and the lossless solution is then obtained by making the loss vanishingly small [24, p. 59] (see Figure 4). For a traditional medium, the branch in (20) is taken such that $\Re e(k_{iz})$ is positive and $\Im m(k_{iz})$ is positive. Figure 5 shows the snap shot of the
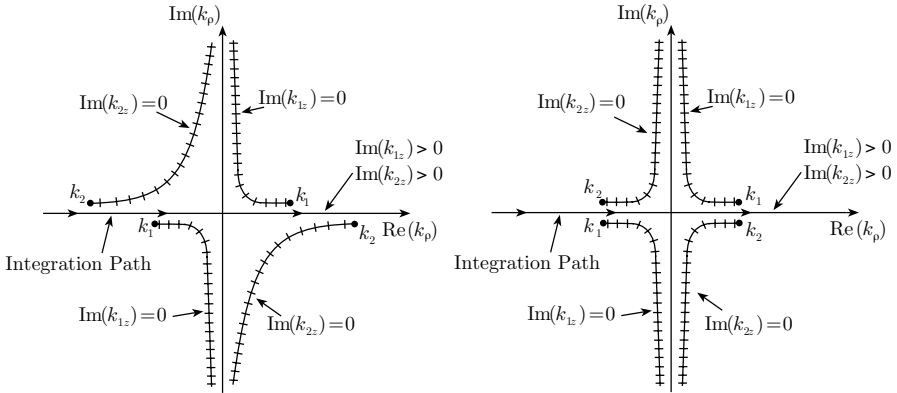
Figure 4. The branch cuts and Riemann sheets for a point source on top of the lossy RHM/LHM half spaces, (left) unmatched case and (right) matched case. $\Re e(k_{1z}) > 0$, $\Re e(k_{2z}) < 0$ on the integration path. For 2D problems, the integration path is from $-\infty$ to $+\infty$, while for 3D problems as in this paper, it is from 0 to $+\infty$.
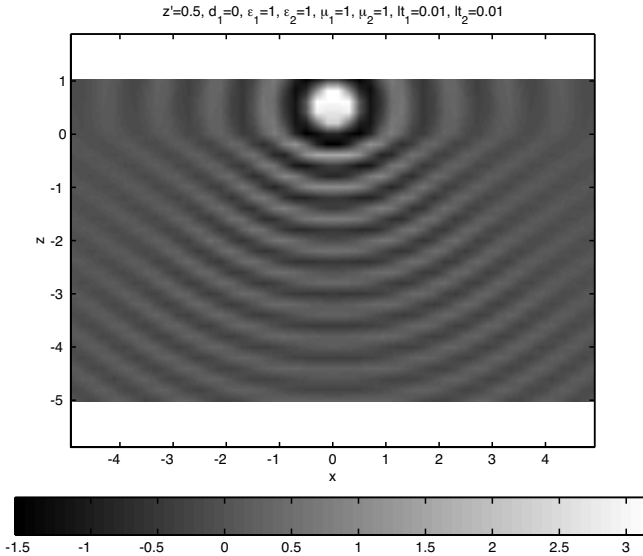

Figure 5. A point source at an ordinary RHM interface generates spherical and lateral waves as seen in this figure [24, p. 109]. x and z are in units of free space wavelengths.

field generated by a point source over an ordinary RHM half space where spherical wave and lateral wave can be observed.

However, if the lower half space is a BWM, the choice of the branch of k_{2z} is such that $\Re e(k_{2z})$ is negative and $\Im m(k_{2z})$ is positive. This will give a backward wave in medium 2 for the propagating spectrum, while ensuring that the wave is decaying in the lower half space for the evanescent spectrum when $z \to -\infty$. The backward wave for the propagating spectrum is for energy conservation, while the decaying wave for the evanescent spectrum is for the convergence of the integral. Consequently, along the integration path, we have the condition that

$$\Im m(k_{1z}) > 0, \quad \Im m(k_{2z}) > 0, \quad \Re e(k_{1z}) > 0, \quad \Re e(k_{2z}) > 0. \quad (21)$$

In the perfectly matched case, as shown in Figure 4 (right), the branch points coalesce to one point, pinching the integration path, making the integral undefined. This is one difficulty we face with the perfectly matched LHM half space. Another difficulty will be discussed in the next section.

8. SURFACE PLASMON RESONANCE

When the lower half space is a single negative material (e.g., where ϵ_2 is negative, but μ_2 is positive), a surface plasmon pole exists along the path of integration [24, p. 100], because the reflection coefficient defined in (19) can have poles when its denominator vanishes or

$$\epsilon_2 k_{1z} + \epsilon_1 k_{2z} = 0 \quad (22)$$

We shall call this the plasmon resonance condition. This surface plasmon mode gives rise to a surface wave that decays exponentially away from the interface. Figure 6 shows the location of such a pole on the complex plane. The above condition differs from the Brewster-angle condition which is

$$\epsilon_2 k_{1z} - \epsilon_1 k_{2z} = 0 \quad (23)$$

When the lower half space is an LHM in addition to being a BWM, there are two cases to consider: the unmatched case, and the matched case. For the unmatched case, where $\mu_2 \neq -\mu_0$ and $\epsilon_2 \neq -\epsilon_0$, the above integral in the lower half space will converge due to the decay of the evanescent waves. As for the pole locations, when $k_\rho < k_i$, $i = 1, 2$, the plasmon resonance condition in Equation (22) cannot be satisfied along the path of integration, and a closer study shows that the poles are located where the Sommerfeld poles or the Zenneck surface wave poles are located. These poles have caused quite a bit of controversy in
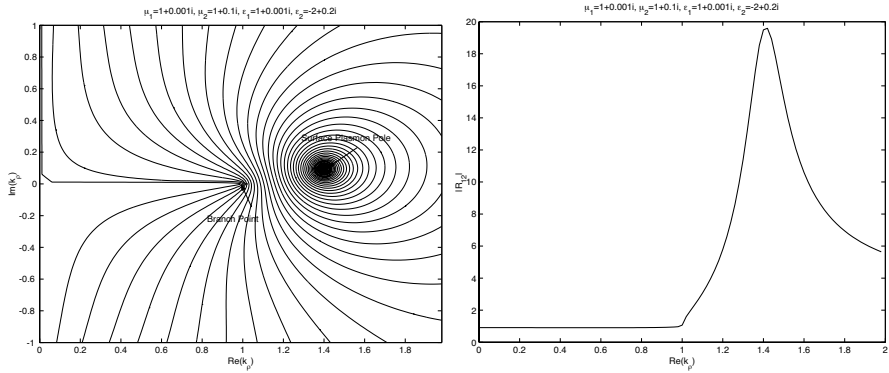
Figure 6. (Left) The contour plot of the magnitude of the reflection coefficient for a single negative material for the lower half space. A pole corresponding to the surface plasmon mode is observed. A branch point is on the real axis while the other branch point is on the imaginary axis [p. 100] [24]. (Right) Plot of the reflection coefficient magnitude along the real axis showing peaking near the pole. Here, $\omega = \mu_0 = \epsilon_0 = 1$.

the literature [25], but they are located in the part of the complex plane topologically far from the integration path, namely, in the "wrong" Riemann sheets. As discussed in [24, p. 99], these poles are located only on two of the four Riemann sheets.

Figure 7 shows the locations of the poles for the unmatched case. They again occur on two Riemann sheets, one is close to the top shore of the $\Im m(k_{1z}) = 0$ branch cut near the real axis, and the other one is close to the bottom shore of the $\Im m(k_{2z}) = 0$ branch cut near the real axis. But they are not coincidental with the path of integration.

When the lower half-space is tuned to be perfectly matched to the upper half space such that $\mu_2 = -\mu_0$ and $\epsilon_2 = -\epsilon_0$, a strange phenomenon occurs. For the propagating wave in the above integral that corresponds to $k_\rho < k$, the reflection coefficient is zero while the transmission coefficient is one. On the contrary, for the evanescent wave corresponding to $k_\rho > k$ with the choice of branch cut suggested above, the reflection coefficient is infinite and the transmission coefficient is infinite for all the evanescent waves due to the denominator of the reflection coefficient defined in (19) becoming zero. This is because the evanescent waves satisfy the surface plasmon resonance condition at the interface given by (22). Hence, in the perfectly matched case, every evanescent wave component excites its corresponding surface plasmon mode. For the lossless case, the Q's of
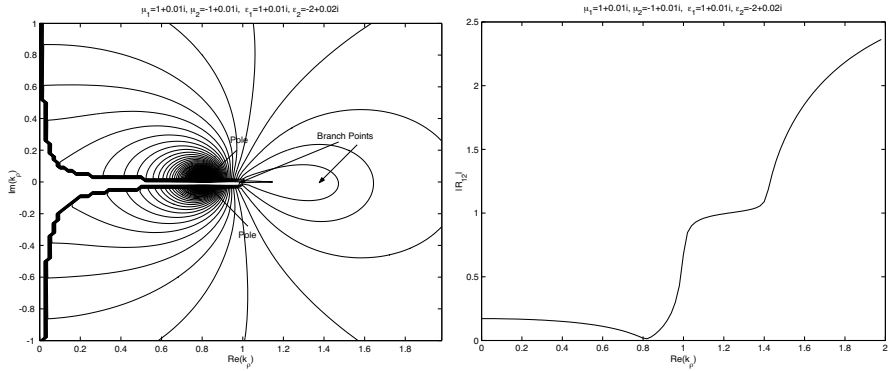
Figure 7. (Left) The contour plot of the magnitude of the reflection coefficient for an unmatched double negative material for the lower half space. Two poles are observed. (Right) Reflection coefficient plot along the real axis shows no large values along the real axis. Here, $\omega = \mu_0 = \epsilon_0 = 1$.

these surface plasmon modes are infinite, and hence, a time-harmonic oscillation will drive their fields to infinity. (This is the second difficulty we face with the LHM half space solution.) Therefore, for the lossless, perfectly matched case, the Sommerfeld integral becomes undefined, and it is well defined only if a small amount of loss is introduced. Figure 8 shows the amplification of the reflected and transmitted evanescent field by a surface plasmon resonance. An evanescent field with unit amplitude is generated at $z = 0$, but when the loss in the LHM becomes smaller, the reflected field swamps the source field.

When the medium is slightly lossy, Figure 9 shows the location of the poles where the plasmon resonance condition is exactly satisfied, and that the plasmon resonance condition is almost satisfied by the evanescent spectrum. When the amount of loss diminishes, the plasmon resonance condition (22) is even better satisfied by the evanescent waves, making the reflection coefficient even larger for $k_\rho > k$. On the other hand, the propagating spectrum satisfies the Brewster angle condition (23) making the reflection coefficient vanishingly small for $k_\rho < k$.

We may wonder if the other choice of square root for k_{2z} for the evanescent wave would have avoided this problem. In this case, the reflection coefficient is zero for the perfectly matched case, and the transmission coefficient is one. The evanescent wave, however, will grow with distance away from the interface giving rise a nonphysical solution and to a divergent integral.
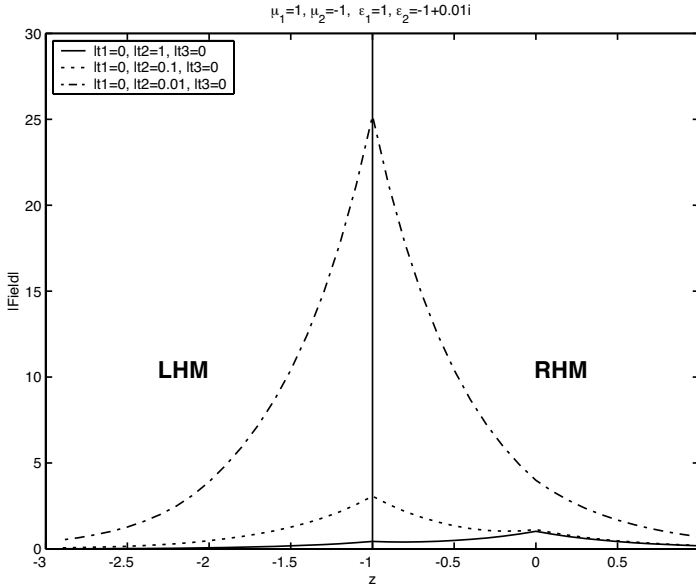
Figure 8. The total (incident and reflected) evanescent field for an interface with plasmon resonance. The lower the loss, the larger the reflected and transmitted field. The source at $z = 0$ generates the evanescent wave with unit amplitude and the interface is at $z = -1$.
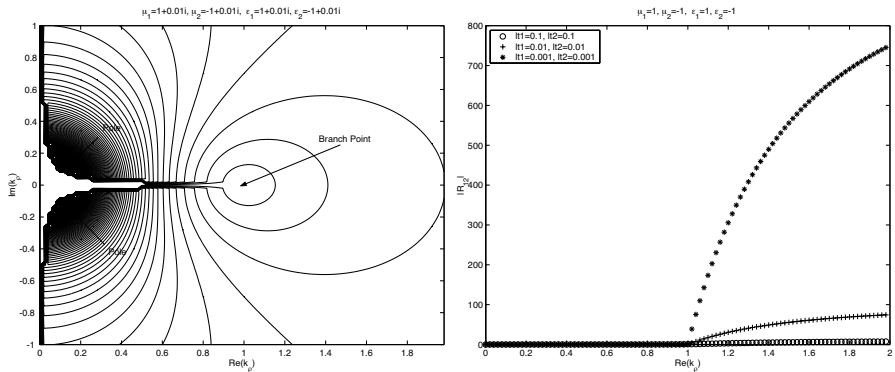

Figure 9. (Left) The contour plot of the magnitude of the reflection coefficient for a matched double negative material for the lower half space. Two poles are observed, and the two branch points almost coalesce into one branch point. (Right) Reflection coefficient plot along the real axes shows large values for evanescent spectrum (to the right of the branch point) for different loss tangents. $\omega = \mu_0 = \epsilon_0 = 1$.
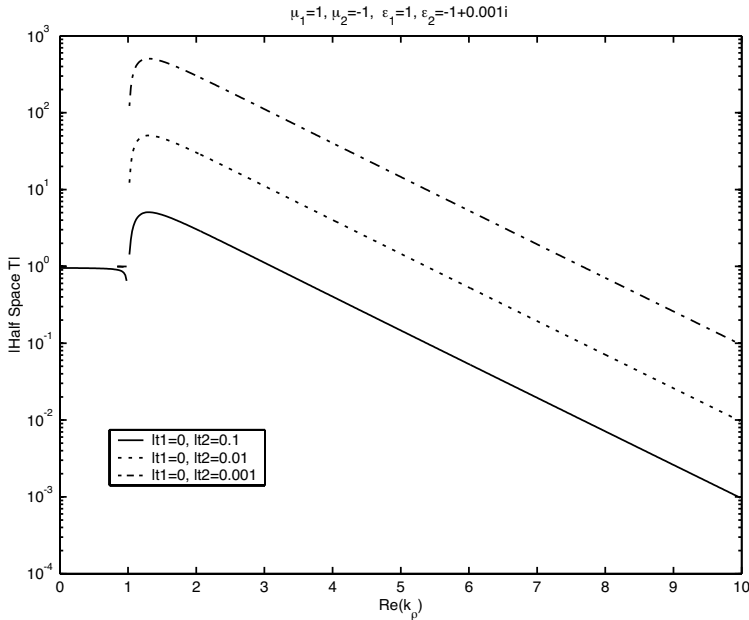
Figure 10. The transmitted field through a matched LHM half space at at distance h = 1 below the interface for different losses. $\omega = \mu_0 = \epsilon_0 = 1$.

From the above, we can also see that the perfectly matched LHM half space does not time-reverse the evanescent wave, but only the propagating wave. The lossless case give rise to nonphysical infinite amplitude surface plasmon resonances yielding infinite field in the lower half space, while the lossy case can be made to amplify the evanescent spectrum through plasmon resonance, but it will not be amplified in the right proportion (see Figure 10) to yield the exact replication of the evanescent wave at the focal point. Hence, super-resolution cannot be achieved in this case.

9. ASYMPTOTIC ANALYSIS–RAY OPTICS SOLUTION

With an analytic solution such as a Sommerfeld integral, one can perform asymptotic analysis using methods such as the stationary phase method (or the saddle point method) on the integral when the frequency is high to obtain ray optics solution to the integrals.

Assume that the source point is at the origin, and is at a height h_1 above the interface. Then for an observation point at a distance h_2
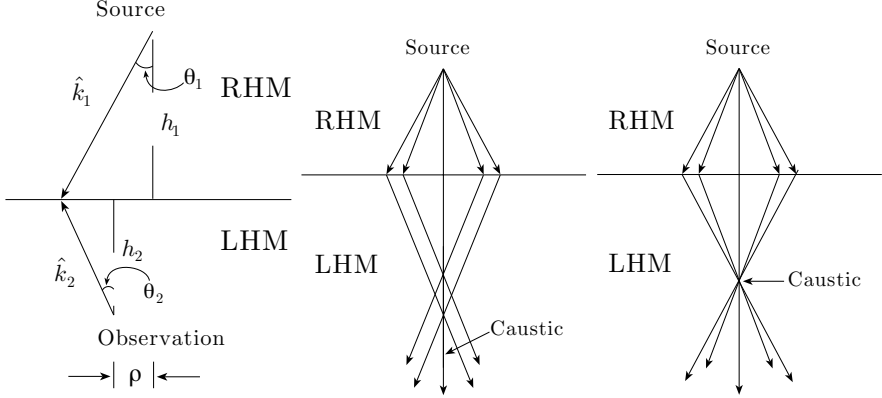
Figure 11. (Left) The parameters for the condition given by Equation (24) for focussing. The rays for the unmatched case (center) form a caustic along the vertical z axis while the rays for the matched case (right) form a caustic at the focal point.

below the interface displaced ρ horizontally away from the origin, one can show that the stationary-phase condition is:

$$-h_1 \tan \theta_1 + h + 2 \tan \theta_2 + \rho = 0 \qquad (24)$$

The relationship between θ_1 and θ_2 is determined by phase matching, or Snell's law (see Figure 11). When the medium is unmatched, $\theta_1 \neq \theta_2$ and the refracted rays will not meet at a point. However, the refracted rays will form a convergent cone toward any point giving rise to a low order caustic (see Figure 11). The field will be infinite at the caustic, but this is due to the well-known mathematical failure of the geometrical optics approximation at caustics, but not due to the focussing effect.

For the matched case, assuming that the surface plasmon resonances are mitigated by some loss, the propagating spectrum will be focussed at a focal point giving rise to a caustic. Again the infinite field at the focal point is a mathematical deficiency rather than a physical reality.

Figure 12 shows the Sommerfeld integral modeling of a point source over an unmatched LHM half space, and over a matched LHM half space. In the first case, there is no focal point, and the field is unfocussed but generating a larger field along the caustic, while in the latter, partial focussing occurs at the focal point.
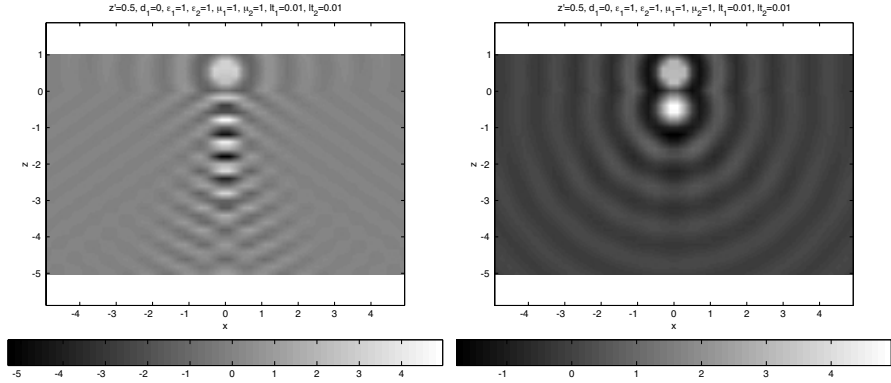
Figure 12. A point source above an LHM half space. (Left) The unmatched case gives rise to unfocussed wave along a caustic. (Right) The matched case gives rise to a partially focussed wave as the evanescent spectrum is not "time-reversed" even though the propagating spectrum is "time-reversed". Dimensions are in free-space wavelength. The source field is clipped at 3 to emphasize the other field.

10. POINT SOURCE OVER AN LHM SLAB

When a vertical electric dipole is placed over an LHM slab, the field in each region can be derived. The field in the upper half space in region 1 is

$$E_{1z} = -\frac{I\ell}{4\pi\epsilon_1} \int_0^\infty dk_\rho \frac{k_\rho^3}{k_{1z}} J_0(k_\rho\rho) \left[e^{ik_{1z}|z-z'|} + \tilde{R}e^{ik_{1z}(z+d_1+|d_1+z'|)} \right] \tag{25}$$

In the slab region, or region 2, the field is

$$E_{2z} = -\frac{I\ell}{4\pi\epsilon_1} \int_0^\infty dk_\rho \frac{k_\rho^3}{k_{1z}} J_0(k_\rho\rho) \left[Ae^{ik_{2z}z} + Be^{-ik_{2z}z} \right] \tag{26}$$

In the lower half space, or region 3, the field is:

$$E_{3z} = -\frac{I\ell}{4\pi\epsilon_1} \int_0^\infty dk_\rho \frac{k_\rho^3}{k_{1z}} J_0(k_\rho\rho)\tilde{T}e^{ik_{1z}|d_1+z'|-ik_{3z}(z+d_2)} \tag{27}$$

In the above [23, 24],

$$\tilde{R} = R_{12} + \frac{T_{12}T_{21}R_{23}e^{2ik_{2z}h}}{1 - R_{21}R_{23}e^{2ik_{2z}h}} = \frac{R_{12} + R_{23}e^{2ik_{2z}h}}{1 - R_{21}R_{23}e^{2ik_{2z}h}} \tag{28}$$

$$\tilde{T} = \frac{T_{12}T_{23}e^{2ik_{2z}h}}{1 - R_{21}R_{23}e^{2ik_{2z}h}} \qquad (29)$$

where the interfaces are located at $z = -d_1$ and $z = -d_2$, h is the slab thickness, and

$$R_{ij} = \frac{\epsilon_j k_{iz} - \epsilon_i k_{jz}}{\epsilon_j k_{iz} + \epsilon_i k_{jz}}; \qquad T_{ij} = 1 + R_{ij} \qquad (30)$$

The detail definitions of A and B are given in reference [24, p. 50] and is unimportant for the following discussion.

As is well known with a slab solution, it is independent of the choice of the square root for k_{2z}. An interesting case to notice here is that for the perfectly matched case, the value of $\tilde{T}$ remains finite, and the value of $\tilde{R} = 0$.

For the propagating spectrum, we always have $\tilde{T}$ reducing to

$$\tilde{T} \to e^{ik_{2z}h}, \qquad \Re e(k_{2z}) < 0 \qquad (31)$$

for the perfectly matched case irrespective of the choice of the square root for k_{2z}. Different choices of square root will yield $R_{ij} = 0$ or $R_{ij} = \infty$ giving rise to the same result above. In other words, the LHM slab regresses the phase of the propagating spectrum, as is expected of a backward wave medium. This is not a surprising result, as we have seen in the half-space analysis that the LHM "time-reverses" the propagating wave.

For the evanescent spectrum, due to the absence of branch point at k_2, by letting $k_{2z} = \pm i\alpha$ always results in

$$\tilde{T} \to e^{\alpha h} \qquad \alpha > 0 \qquad (32)$$

Moreover, the reflection coefficient, which was infinite for the half-space case, becomes zero for this case, and the transmission coefficient remains a finite value. This is a surprising departure from the LHM half space — an LHM slab amplifies the evanescent spectrum. Hence, with a proper choice of the LHM slab thickness, such that the slab thickness is exactly the same as the height of the point source above the slab, the decay of the evanescent field can be exactly compensated by the LHM slab, and the phase progression of the propagating wave can be exactly compensated by the phase regression in the LHM slab. (Such amplification has also been found in circuit equivalence models [17, 20].)

The above is a case of resonance tunnelling. As mentioned in the half-space analysis, the evanescent spectrum satisfies the plasmon resonance condition, generating infinities in the one-interface reflection
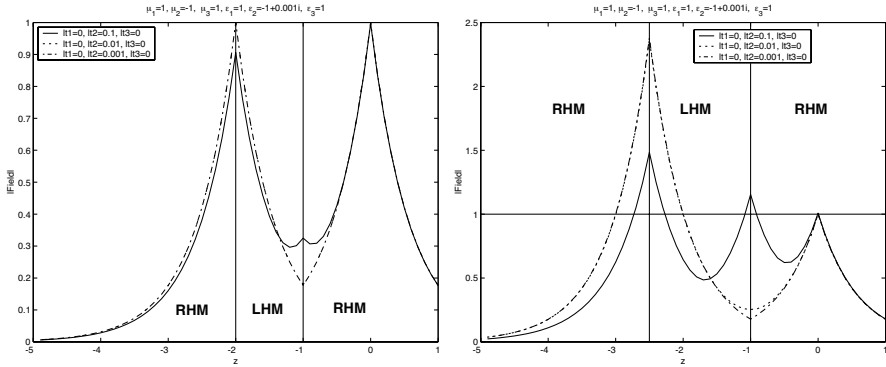
Figure 13. The propagation of the plane evanescent field from the source point at $z = 0$ into a thin LHM slab (left) and thick LHM slab (right).

and transmission coefficients. These resonances at the two interfaces interact with each other to yield a saturated field in the slab region, giving rise to no reflection, and amplification of the transmitted field.

As seen in Figure 13, a plane evanescent field in an RHM region decays away from the source point, and when it enters the LHM slab, the evanescent field experiences an exponential growth due to resonance coupling between the two interfaces, and the field is amplified by the slab. As the evanescent field leaves the slab, it decays again from the slab. As can be seen from the figure, the reflected evanescent field decreases for decreasing loss because of better matching, and in the limit of very small loss, the field can replicate itself at $z = -2$ for the thin slab. For the thick slab, the field is replicated at $z = -2$ inside the slab and at $z = -3$ outside the slab. For the lossy case, considerable more reflected wave is observed in the thick slab.

11. SUPER-RESOLUTION ANALYSIS

To gain further insight into the super-resolution nature of an LHM slab, we can study the contour plot of the generalized transmission and reflection coefficients on the complex plane in Figures 14 and 15. The contour plot indicates no poles, save for the branch point. The transmission coefficient is large at the right half of the figure, while the reflection coefficient also becomes larger. The next set of figures reveal more on the character of these transmission and reflection coefficients.

Figure 16 shows the magnitude of the generalize transmission and reflection coefficients given by (29) and (28) for the LHM slab as a
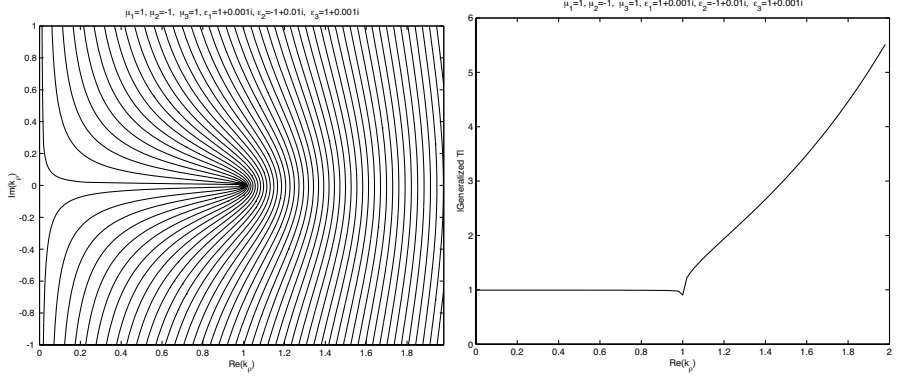
Figure 14. The contour plot of the magnitude of the LHM slab transmission coefficient (left) and the same coefficient along the real axis (right). Here, $\omega = \mu_0 = \epsilon_0 = h = 1$.
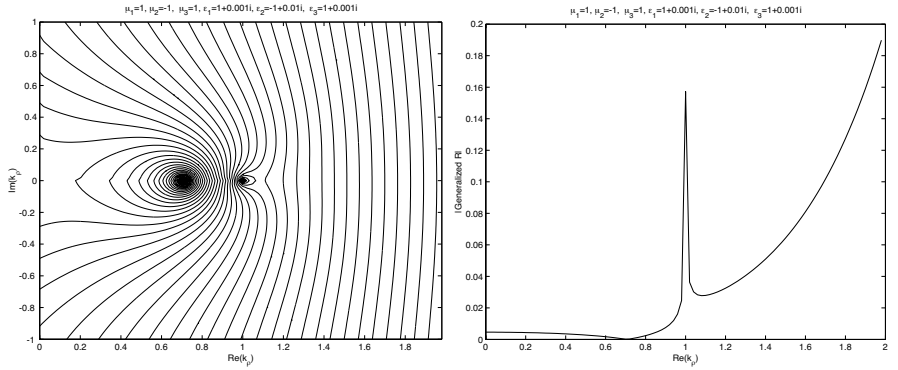

Figure 15. The contour plot of the magnitude of the LHM slab reflection coefficient (left) and the same coefficient along the real axis (right). Here, $\omega = \mu_0 = \epsilon_0 = h = 1$.

function of k_ρ for different loss tangents of the slab. The transmitted evanescent spectrum $(k_\rho > k)$ is amplified by the slab up to some $k_{\rho max}$ where the transmission coefficient is maximum. After that the transmission coefficient diminishes and the amount of amplification depends on the loss in the slab-the more loss, the less the amplification. Meanwhile, the reflection coefficient, which is small, becomes large for large k_ρ implying that the high spatial frequency evanescent spectrum cannot penetrate the LHM slab.

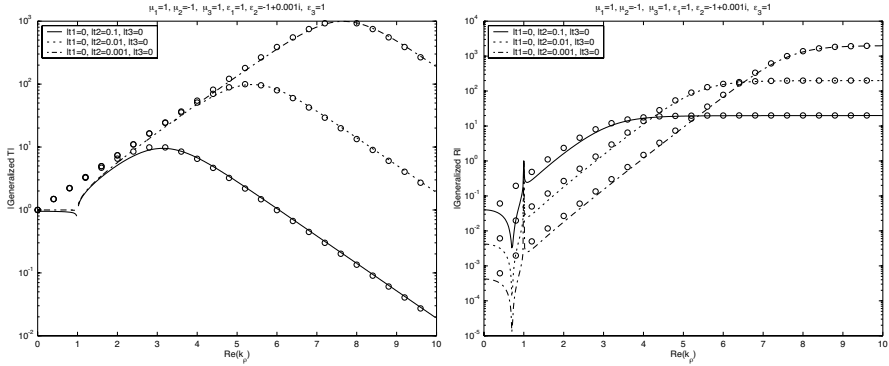When k_ρ is large, the generalized transmission coefficient (29) can

Figure 16. The magnitude of the LHM slab transmission coefficient (left) and reflection coefficient (right) along the real axis integration path for decreasing loss tangents. The circles are the asymptotic approximation to the formula for large k_ρ. Here, $\omega = \mu_0 = \epsilon_0 = h = 1$.

be approximated by

$$\tilde{T} \sim \frac{(1 - r_{12})(1 - r_{23})e^{-k_\rho h}}{1 - r_{21}r_{23}e^{-2k_\rho h}}, \quad k_\rho \to \infty \tag{33}$$

where

$$r_{ij} = \frac{\epsilon_j - \epsilon_i}{\epsilon_j + \epsilon_i} \tag{34}$$

The above equation, and a similar equation for the reflection coefficient, are plotted as circles in Figure 16. For the matched interface with small loss,

$$r_{ij} = -\frac{2}{i(l_{t1} + l_{t2})} \tag{35}$$

where l_{ti} is the loss tangent of medium i. With the above approximations, we can derive

$$k_{\rho max} \approx \frac{1}{h} \ln(|r_{12}|) \approx \frac{1}{h} \ln(2/(l_{t1} + l_{t2})) \tag{36}$$

Hence, the minimum spatial wavelength that can be regenerated by the RHM slab is

$$\lambda_{min} = 2\pi h / \ln(2/(l_{t1} + l_{t2})) = 2\pi h / \ln(2/(l_{t2})), \quad \text{if } l_{t1} = 0. \tag{37}$$

The resolution of an image is about $0.5\lambda_{min}$. Hence, super-resolution is possible where the resolution is controlled by the thickness and the
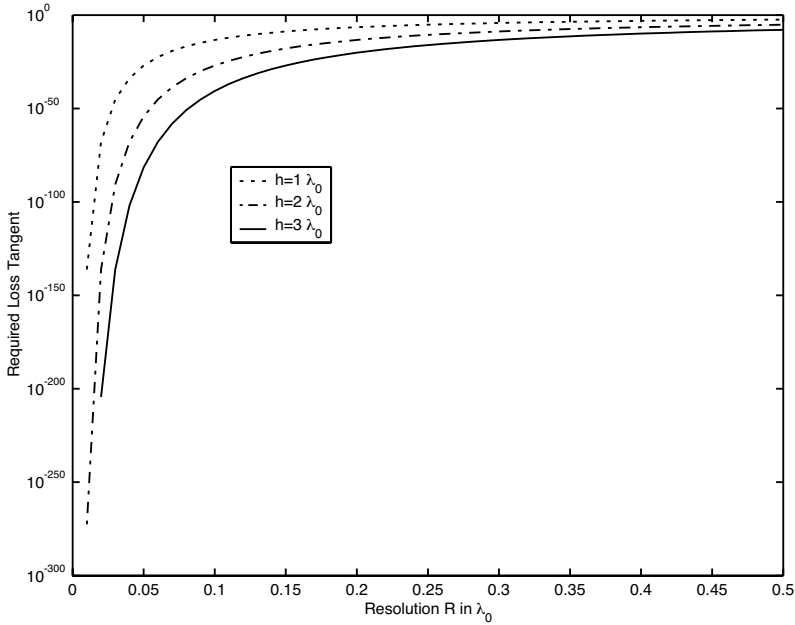
Figure 17. Required loss tangent of the LHM slab versus resolution in wavelength for different slab thicknesses.

loss of the LHM slab. Defining the resolution $R = 0.5\lambda_{min}$, obtain that

$$l_{t1} = 2e^{-\pi h/R} \tag{38}$$

Figure 17 shows the required loss tangent for the LHM slab for resolution in terms of free-space wavelength for different slab thicknesses. It is seen that when the resolution is small, and the slab thickness is large, the required loss tangent is very small! To put things in perspective, an optical fiber with a loss of $0.5\,\mathrm{dB/km}$ at $1.6\,\mu\mathrm{m}$ wavelength requires a loss tangent of approximately 3×10^{-11}.

Since an deep evanescent field (large k_ρ) becomes exponentially small when it reaches the LHM slab interface, before it is amplified, any surface imperfection or roughness will also limit the super-resolving capability of the slab. The above analysis has not taken this into account.

Figure 18 shows the use of an LHM slab properly placed and with thickness selected so that the field due to the source is refocussed exactly at the point at the bottom interface of the slab. For the thin slab, a hot spot is refocussed at the bottom interface of the slab at
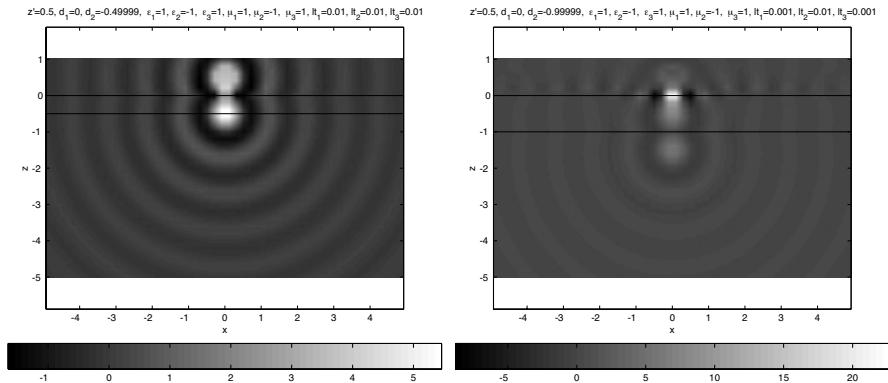
Figure 18. Contour plot of a snap shot of the field magnitude for a point source above an LHM slab. The source is placed at $(\rho, z) = (0., 0.5)$ above the slab. The LHM slab is matched and has a thickness of 0.5 (left) and 1.0 (right). Dimensions are in wavelength. The source field is clipped at 3 to emphasize the other field.

$(\rho, z) = (0., -0.5)$. The source field at $(\rho, z) = (0., 0.5)$ is clipped at 3 to limit its value.

For the thick slab, a hot spot is refocussed inside the LHM slab, as well as one below the LHM slab. Also, a hot spot is noticed at the top interface directly below the source point. This is due to that the high spatial frequency evanescent spectrum cannot penetrate the slab (see Figure 16), giving rise to accumulation of field for this hot spot.

The above result suggests that an LHM slab can "teleport" a point source to a new location where the point source is reconstituted to beyond the diffraction limit. Supposedly, such a slab can be used to teleport an illuminated planar image to another plane that allows sub-wavelength features to be captured without having to perform near field scanning microscopy directly. However, an extremely high Q or low loss slab is needed to achieve such a teleportation. One possibility is the use of active material to counter the loss in the LHM slab.

12. CONCLUSIONS

Some reflections on the physical character of double negative, left handed medium is given in this paper. In particular, we perform theoretical modelling with Sommerfeld integral to gain a better physical insight into the interaction of a point source (that generates both propagating waves and evanescent waves) with an LHM half space

and an LHM slab. Loss condition has been derived for LHM so that it can be used to decide the choice of Riemann sheets for the Sommerfeld integration path. Consequently, a more precise understanding of the problem can be gained compared to FDTD simulations.

This analysis shows that an LHM half space cannot refocus the point source field to super-resolution, because the evanescent spectrum is not reconstituted in the correct proportion. A lossless LHM dielectric slab can refocus the field to super-resolution if the point source is properly located with respect to the slab; namely, the thickness of the LHM slab is exactly the same as or larger than the distance of the point source above the slab. If the slab thickness is exactly the same as this distance, the point source is refocussed at the point directly at the bottom interface to high resolution. If the thickness of the slab is larger than the distance of the dipole from the interface, it can refocus the point source to a point below the dielectric slab, but a very low loss LHM slab is needed for such a purpose. However, the super-resolution is limited by the loss of the LHM slab. In fact, the loss in the dielectric slab causes the high spatial frequency evanescent field to be reflected, giving rise to hot spots at the dielectric interface. This analysis also clarifies confusions about the time-reversal super-resolution capabilities of LHM.

Furthermore, we suggest that high-resolution teleportation is possible with a layered medium consisting of alternating RHM and LHM materials although it will be limited by the loss in the LHM slab. A pressing requirement in this field is the fabrication of novel LHM with very low loss, or the study of the use of active material to counter the loss in the LHM slab.

REFERENCES

1. Veselago, V. G., "The electrodynamics of substances with simultaneously negative values of permittivity and permeability," *Soviet Physics USPEKI*, Vol. 10, 509, 1968.

2. Pendry, J. B., "Negative refraction makes a perfect lens," *Phys. Rev. Lett.*, Vol. 85, 3966, 2000.

3. Smith, D. R., W. J. Padilla, D. C. Vier, S. C. Nemat-Nasser, and S. Schultz, "Composite medium with simultaneously negative permeability and permittivity," *Phys. Rev. Lett.*, Vol. 84, 4184, May 1, 2000.

4. Smith, D. R. and N. Kroll, "Negative refractive index in left-handed material," *Phys. Rev. Lett.*, Vol. 85, 2933, Oct. 2, 2000.

5. Lindell, I. V., S. A. Tretyakov, K. I. Nikoskinen, and S. Ilvonen,

"BW mediamedia with negative parameters, capable of supporting backward waves," *Microwave and Optical Technology Letters*, Vol. 31, No. 2, 129–133, 2001.

6. Caloz, C., C.-C. Chang, and T. Itoh, "Full-wave verification of the fundamental properties of left-handed materials in waveguide configurations," *Journal of Applied Physics*, Vol. 90, Issue 11, 5483–5486, 2001.

7. Ruppin, R., "Extinction properties of a sphere with negative permittivity and permeability," *Solid State Communications*, Vol. 116, 411–415, Oct. 20, 2000.

8. Ziolkowski, R. W., "Superluminal transmission of information through an electromagnetic metamaterial," *Physical Review E*, Vol. 63, 046604, 2001.

9. Shelby, R. A., D. R. Smith, S. C. Nemat-Nasser, and S. Schultz, "Microwave transmission through a two-dimensional, isotropic, left-handed metamaterial," *Applied Physics Letters*, Vol. 78, Issue 4, 489–491, Jan. 22, 2001.

10. Ziolkowski, R. W. and E. Heyman, "Wave propagation in media having negative permittivity and permeability," *Physical Review E*, Vol. 64, 056625, 2001.

11. Sarychev, K., V. M. Shalaev, and V. A. Podolskiy, "Plasmon modes in metal nanowires and left-handed materials," *Journal of Nonlinear Optical Physics & Materials*, Vol. 11, No. 1, 65–74, 2002.

12. Pendry, J. B. and S. Anantha Ramakrishna, "Near-field lenses in two dimensions," *Journal of Physics: Condensed Matter*, Vol. 14, 8463–8479, 2002.

13. Eleftheriades, G. V., A. K. Iyer, and P. C. Kremer, "Planar negative refractive Index media using periodically L-C loaded transmission lines," *IEEE Trans. on Microwave Theory and Tech.*, Vol. 50, No. 12, 2702–2712, Dec. 2002.

14. Pacheco Jr., J., T. M. Grzegorczyk, B.-I. Wu, Y. Zhang, and J. A. Kong, "Power propagation in homogeneous isotropic frequency dispersive left-handed media," *Physical Review Letters*, Vol. 89, 257401, Dec. 16, 2002.

15. Kong, J. A., B.-I. Wu, and Y. Zhang, "A unique lateral displacement of a Gaussian beam transmitted through a slab with negative permittivity and permeability," *Microwave and Optical Technology Letters*, Vol. 33, No. 2, 137–139, April 20, 2002,

16. Engheta, N., "An idea for thin subwavelength cavity resonators using metamaterials with negative permittivity and permeability,"

   IEEE Antennas and Wireless Propagation Letters, Vol. 1, No. 1, 10–13, 2002.

17. Grbic, A. and G. V. Eleftheriades, "Growing evanescent waves in negative-refractive-index transmission-line media," *Applied Physics Letters*, Vol. 82, Issue 12, 1815–1817, March 24, 2003.

18. Smith, D. R., D. Schurig, M. Rosenbluth, S. Schultz, S. Anantha Ramakrishna, and J. B. Pendry, "Limitations on subdiffraction imaging with a negative refractive index slab," *Applied Physics Letters*, Vo. 82, Issue 10, 1506–1508, March 10, 2003.

19. Loschialpo, P. F., D. L. Smith, D. W. Forester, F. J. Rachford, and J. Schelleng, "Electromagnetic waves focused by a negative-index planar lens," *Phys. Rev. E*, Vol. 67, 025602, 2003.

20. Alu, A. and N. Engheta, "Circuit equivalence of 'growing exponential' in Pendry's lens," *USNC/CNC/URSI North American Radio Science Meeting Digest*, 22, Columbus, OH, June 22–27, 2003.

21. Feynman, R., R. B. Leighton, and M. L. Sands, *The Feynman Lectures on Physics*, Vol. I, Chapter 52, Addison-Wesley Publishing Co., 1965.

22. Lee, T. D. and C. N. Yang, "Question of parity conservation in weak interaction," *Phys. Rev.*, Vol. 104, No. 1, 254–257, 1956.

23. Kong, J. A., *Electromagnetic Wave Theory*, John Wiley & Sons, New York, 1990.

24. Chew, W. C., *Waves and Fields in Inhomogeneous Media*, Van Nostrand Reinhold, New York, 1990. Reprinted by IEEE Press, 1995.

25. Banõs, Jr., A., *Dipole Radiation in the Presence of a Conducting Half-Space*, Pergamom Press, New York, 1966.

W. C. Chew Founder Professor, College of Engineering, and Electrical and Computer Engineering, has taught at Illinois since 1985. He conducts research in fast algorithms for solving scattering problems, inverse scattering, geophysical sensing, NDE, and super-resolution experiments. He has supervised 20 Ph.D. theses and 23 master's theses, and published over 250 journal papers. He has received the NSF Presidential Young Investigator Award (1986), the IEEE Graduate Teaching Award (2000), and the Campus Award for Excellence in Graduate and Professional Teaching (2001). He is a Fellow of the IEEE and the Optical Society of America, and a Most-Highly Cited Author with ISI.